Forestry: An International Journal of Forest Research, 2023, 1–17
https://doi.org/10.1093/forestry/cpad055
Original Article

Predicting net growth rates in boreal forests using Landsat time series and permanent sample plot data

Alexandre Morin-Bernard [1,*], Nicholas C. Coops[2], Joanne C. White[3] and Alexis Achim[1]

[1]Department of Wood and Forest Sciences, Université Laval, 2405 rue de la Terrasse, Québec, QC G1V 0A6, Canada
[2]Department of Forest Resources Management, University of British Columbia, 2424 Main Mall, Vancouver, BC V6T 1Z4, Canada
[3]Canadian Forest Service (Pacific Forestry Centre), Natural Resources Canada, 506 West Burnside Road, Victoria, BC V8Z 1M5, Canada
*Corresponding author. Tel: +1 418 6563025; E-mail: alexandre.morin-bernard@sbf.ulaval.ca

Abstract

Increasing temperature and changes in water dynamics are bringing uncertainty regarding the future productivity of boreal forests, even in the absence of stand-replacing disturbances. There is accumulating evidence that water deficits caused by warmer summer temperatures are linked to decreases in the growth rate of boreal tree species in some regions. In this context, it is essential to provide forest professionals with a means of monitoring net forest growth rates in undisturbed areas and at the scale of a management unit in order to determine where and when changes in growth are taking place. This is challenging using conventional forest inventory approaches. In this study, we use Landsat time series and data from permanent sample plots (PSP) to develop spatially explicit estimates of annual net basal area growth at a 30-m spatial resolution for a forest management unit in Canada. An ordinary least square regression model was developed using data from 120 PSPs and validated on an independent set of 60 PSPs, with R^2 values of 0.61 and 0.58, respectively. Applying the model over a 586 607-ha study area revealed considerable temporal and spatial variability in the predicted growth rates and their evolution through time. There was an overall decline in predicted growth rates over time, with this trend corroborated by the PSP data and attributed to the ageing demographics of the forests in the study area. This variability was related to forest development stage, species composition, and structural attributes derived from light detection and ranging (LiDAR). The information generated by the suggested approach can help to improve yield predictions, optimize rotation lengths, and allow for the identification of target areas where silvicultural interventions aimed at maintaining or enhancing growth could be conducted.

Keywords: boreal; Landsat; time series; forest growth; LiDAR; black spruce

Introduction

Boreal forests are amongst the largest ecosystems on earth (Brandt *et al.* 2013) and contain a third of the global terrestrial biogenic carbon stock (Pan *et al.* 2011). A large part of the boreal forest biome hosts management activities that account for a third of the lumber produced worldwide (Gauthier *et al.* 2015). In Canada, ~70% of the forest extent lies within the boreal zone, with the contiguous boreal forest covering a total area of 270 Mha (Brandt *et al.* 2013). This geographical extent makes it a particularly challenging ecosystem to manage, especially in the context of climate change. In particular, increasing rates of disturbances and tree mortality (Peng *et al.* 2011; Seidl *et al.* 2017) as well as increasing temperature and changes in water dynamics will alter the growth response of boreal forests (D'Orangeville *et al.* 2018; Girardin *et al.* 2016b), bringing uncertainty regarding their future productivity.

Although boreal tree species can benefit from a lengthening of the growth season and increased CO_2 levels (D'Orangeville *et al.* 2018; Subedi and Sharma 2013), the rapid changes in environmental conditions may be outpacing the ability of species to adapt, which could result in forested ecosystems where the species composition is no longer in equilibrium with the climate (Huang *et al.* 2010). There is accumulating evidence that warmer summer temperatures are causing increased water deficits in some regions, linked to decreases in the growth rate of black spruce [*Picea mariana* (Mill.) B.S.P.], the most abundant tree species in the boreal zone (Chagnon *et al.* 2022; D'Orangeville *et al.* 2018; Girardin *et al.* 2016b). The accumulation of drought events have already caused increased mortality rates in black spruce forests (Peng *et al.* 2011; Sánchez-Pinillos *et al.* 2022). Jack pine (*Pinus banksiana* Lamb), a fire-adapted species known for colonizing xeric sites, has also experienced a generalized growth decline in eastern Canada over the last decades, attributed to increased water stress (Dietrich *et al.* 2016; Girardin *et al.* 2012).

Whilst the net aboveground biomass (AGB) of Canada's forested ecosystems increased between 1984 and 2016, growth rates over the undisturbed persistent forests have been highly variable (Wulder *et al.* 2020). Observed changes in growth are influenced by multiple factors such as species composition, stand age and development stage, structural attributes, and site characteristics (Dietrich *et al.* 2016; D'Orangeville *et al.* 2018; Mamet *et al.* 2015; Marchand *et al.* 2019). Understanding what growth changes have already occurred and predicting future changes in this ecosystem is therefore very difficult, but crucial. Reduction in carbon assimilation rates could offset the effect of strategies aiming to increase the forest carbon sink (Kurz *et al.* 2008; Seidl *et al.* 2014) and eventually lead to reductions in the timber supply (Brecka *et al.* 2018; McDowell *et al.* 2020).

Handling editor: Dr. Fabian Fassnacht
Received: May 16, 2023. **Revised:** September 14, 2023. **Accepted:** October 20, 2023

To manage risks associated with the uncertain growth response of trees across the landscape, forest practitioners will increasingly need to rely on adaptive silvicultural actions to promote more resistant and resilient forest stands (Achim et al. 2022; Gardiner and Moore 2014; Moreau et al. 2022). In this context, it is essential to provide forest professionals with a means of monitoring net forest growth in undisturbed areas and at the scale of a management unit in order to determine where and when changes in growth are taking place, which is challenging using conventional forest inventory approaches (Bowman et al. 2013; Gillis et al. 2005).

Remote sensing technologies can provide temporally continuous and spatially contiguous coverage of forest condition. With an analysis-ready image archive dating back to 1984 and a moderate spatial resolution (30 m), the high radiometric and geometric qualities of the Landsat TM, ETM+, and OLI sensors provide a robust basis for the characterization of change in boreal forests at both global and local scales (Sulla-Menashe et al. 2018). These characteristics have made Landsat imagery a primary source of data for characterizing changes in forest condition (Banskota et al. 2014; Wulder et al. 2022). Capitalizing on the known relationships between spectral indices and the physiological responses of trees, several studies have utilized Landsat data to investigate gradual changes in forest productivity (e.g. Vogelmann et al. 2016), model changes in forest biomass dynamics (e.g. Gomez et al. 2015), and identify declining stands (Czerwinski et al. 2014). Whilst satellite imagery allows for the observation of changes over time, light detection and ranging (LiDAR) provides detailed wall-to-wall information on forest structural attributes and development stage (Baltsavias 1999; Lefsky et al. 2002; Wulder et al. 2012). Using LiDAR in combination with satellite imagery has proven useful for extending the spatial and temporal coverage of LiDAR data sets (Matasci et al. 2018; Zald et al. 2016), and offers the possibility to better understand patterns of growth across boreal forests in the last decades and relate them to the existing forest structure, generating useful information for the implementation of efficient, adaptive silvicultural practices (Achim et al. 2022).

Our overall objective was to use Landsat time series data to develop spatially explicit estimates of net basal area growth at a 30-m spatial resolution for a forest management area in Ontario, Canada. We then examined the predicted growth rates in the context of forest development stage, species composition, and structural attributes derived from LiDAR and discuss the potential of the proposed approach to provide relevant information for the implementation of adapted forest management practices.

Methods

The current study comprises several methodological stages that involve relating field measurements of forest growth with variables derived from Landsat data. The annual net growth rate of conifer-dominated stands was first determined using repeated measurement data from permanent sample plots located in the boreal zone of eastern Canada. Subsequently, a model selection approach was used to identify the optimal set of Landsat-derived variables to construct a predictive model for net forest growth. This model was then applied to a forest management unit, which was subdivided into forest-type examples with unique structural attributes using LiDAR data. Model predictions were then examined in relation to forest composition and structure.

Study area

The Romeo Malette Forest (RMF), located in Ontario, Canada (Fig. 1), covers 586 607 ha within the Lake Abitibi ecoregion in the Ontario Shield ecozone (Wester et al. 2018). The main tree species in this forest management unit include black spruce, jack pine, white spruce [*Picea glauca* (Moench) Voss], poplar (*Populus* spp.) and white birch (*Betula papyrifera* Marshall) with components of balsam fir [*Abies balsamea* (L.) Mill], cedar (*Thuya* spp.), Eastern larch [*Larix laricina* (Du Roi) K. Koch], and white and red pines (*Pinus strobus* L. and *Pinus resinosa* Soi ex. Aiton). The area is under active forest management by a sustainable forest license holder. The primary harvested species are black spruce, jack pine, balsam fir, and poplar, for a total harvested volume of 2 935 969 m^3 between 2012 and 2019. The RMF can be considered as a relatively young forest, with, as of 2023, a median age of 78 years, and only 5% of the forested area being older than 133 years of age (Bilyk et al. 2021).

The mean annual temperature in the area is 1.8°C and the area receives 773 mm of precipitation annually, based on the historical mean for the period 1981–2010 extracted from ClimateNA (Wang et al. 2016). The disturbance regime in the study site is characterized by wildfire, windthrow, and insect defoliation mainly from the spruce budworm [*Choristoneura fumiferana* (Clem.)] and forest tent caterpillar (*Malacosoma disstria* Hübner) (Urquizo et al. 2000). By 2050, according to projections made using a 13 global circulation model ensemble and averaged under four shared socioeconomic pathways (i.e. SSPs 1–4) scenarios (Mahony et al. 2022), both the minimum and maximum temperatures are expected to increase by 2.9°C in this region. Warmer summers with no change in precipitation and warmer winters with less precipitation falling as snow could increase the risk of drought and vulnerability to forest pests (Wotherspoon et al. 2022).

Data from permanent sample plots

Data on forest growth were gathered from permanent sample plots located within the RMF and in adjacent forest management units with high densities of PSP (Fig. 1). The 11.28-m-radius (400 m^2) circular plots are part of the network of permanent field plots periodically measured within the growth and yield programme from the Ontario Ministry of Natural Resources and Forestry (Hayden 1995). The current study focused on stands containing the dominant coniferous species in this region. We only selected plots in which >50% of the basal area at the time of the first measurement was composed of black spruce, jack pine, and balsam fir. We also excluded plots in which >20% of the basal area was composed of deciduous species. This threshold was set to avoid spectral inconsistencies due to changes in species composition during the measurement intervals, which are known to generate trends that are not related to forest growth and productivity, but rather to succession or disturbances (Fiore et al. 2020). We initially selected 493 plots that were measured at least twice between 1993 and 2018, from which 169 were excluded due to the mixed species composition. The candidate plots were additionally filtered to exclude all plots that were disturbed during the measurement interval, due to harvesting, silvicultural treatments, or non-stand replacing disturbances. Finally, we ensured that the forest surrounding the plots was homogeneous within a radius of 80 m, resulting in a final number of 180 plots (Fig. 1).

At each plot, the crown class and DBH of every tree with a minimum DBH of 2.5 cm were recorded in accordance with the Ontario growth and yield programme reference manual (MNRF 2016). To derive an estimate of the current growth conditions, we used tree-level measurements from the earliest and latest measurement to calculate the plot-level annual net basal area increment, hereafter referred to as the net growth, in the interval between the visits, which ranged from 5 to 24 years (median of

Table 1. Characteristics of the permanent sample plots included in the development of the model at the time of the first and last field measurements.

	Basal area (m^2 ha^{-1})	Stem density (stem ha^{-1})	Mean DBH (cm)	Composition (% BA)				
				Black spruce	Jack pine	Balsam fir	American larch	Deciduous
First measurement								
Average	22.8	2567	11.5	58.7	79.6	8.0	6.0	2.9
Min	3.2	400	4.4	0.1	0.1	0.1	0.1	0.0
Max	50.4	6925	21.5	100.0	100.0	100.0	39.6	18.1
Last measurement								
Average	27.1	2847	11.7	53.6	74.5	6.4	6.8	3.4
Min	5.8	1000	4.3	0.1	0.0	0.0	0.1	0.0
Max	53.3	7675	21.1	100.0	100.0	78.6	45.5	18.0

Mean DBH corresponds to the root mean square DBH at the plot level.

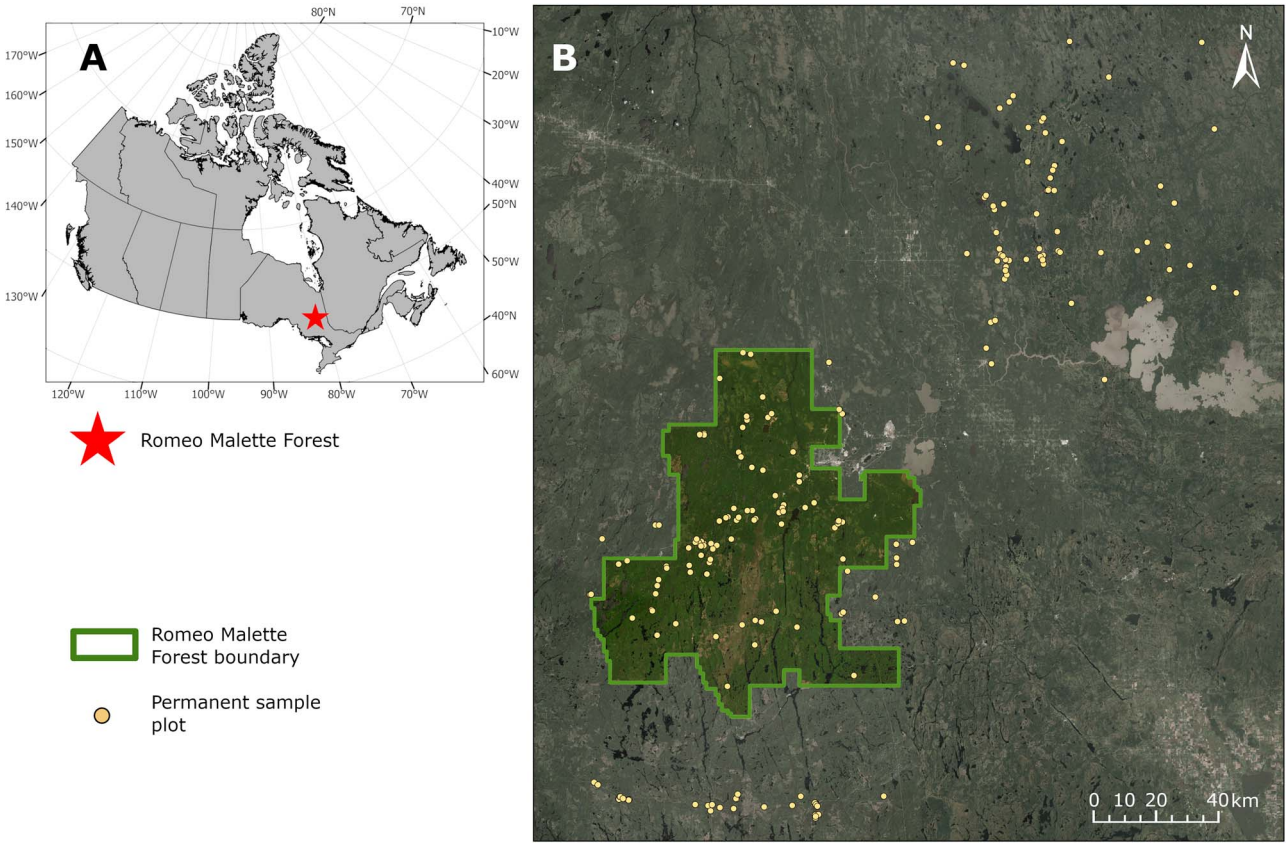

Figure 1. (a) Location of the RMF in Canada. (b) Boundary of the RMF and location of the permanent sample plots used in model development.

10 years). The net growth consists of the basal area growth of trees that survived between the two measurements plus the basal area of trees that reached the DBH threshold of 2.5 cm during the interval, from which we deduce the basal area of trees that died in that same period. A net growth rate in m^2 ha^{-1} yr^{-1} was then calculated for each plot by dividing the net basal area growth by the number of growing seasons between the two field measurements. The median net growth rate measured in the selected plots was 0.52 m^2 ha^{-1} yr^{-1} (standard deviation = 0.38 m^2 ha^{-1} yr^{-1}).

Landsat surface reflectance composite time series

We created annual, gap-free, best-available pixel surface reflectance composites (BAP, White *et al.*, 2014) over the entire study site for the period 1984–2021. BAPs are created from Landsat 5 TM, Landsat 7 ETM+, and Landsat 8 OLI orthorectified and atmospherically corrected surface reflectance images, by selecting the best pixel based on the proximity to a target date, distance to clouds and cloud shadows, atmospheric quality and acquisition sensor, and by subsequently filling data gaps if no valid observation was available for a given pixel (Hermosilla *et al.* 2015; White *et al.* 2014). Only Landsat observations acquired between 1 July and 30 August were used to create the composites.

From the BAP composites, a time series of selected vegetation indices were extracted (VI, Table 2) and averaged over a 3 × 3 pixel window centred over each of the permanent sample plots, for the period corresponding to the interval between the first and last field measurements. This window size was chosen to account for the limited accuracy of the plots' geolocation and ensured that the extracted spectral values would be representative of the actual canopy condition at the plot location. Among the selected vegetation indices for the current study was the normalized burn

Table 2. Vegetation indices, equations, and references used in the current study.

Vegetation index	Equation	Reference
Normalized difference vegetation index (NDVI)	=(NIR − Red)/(NIR + Red)	(Tucker 1979)
Normalized burn ratio (NBR)	=(NIR − SWIR2)/(NIR + SWIR2)	(Key and Benson 2006)
Tasselled cap wetness (TCW)	=0.0315 * Blue + 0.2021 * Green +0.3102 * Red +0.1594 * NIR − 0.6806 * SWIR1 − 0.6109 * SWIR2	(Crist 1985)
Tasselled cap angle (TCA)	= arctan (TCG/TCB) TCG = −0.1603 * Blue − 0.2819 * Green − 0.4934 * Red +0.7940 * NIR − 0.0002 * SWIR1 − 0.1446 * SWIR2 TCB = 0.2043 * Blue +0.4158 * Green +0.5524 * Red +0.5741 * NIR + 0.3124 * SWIR1 + 0.2303 * SWIR2	(Crist 1985; Powell et al. 2010)

ratio (NBR), a normalized difference of the near-infrared (NIR) and second shortwave-infrared Landsat bands (SWIR2) and has been proven useful in monitoring post-disturbance recovery not only after fire but also after harvesting, even in the case of non-stand replacing disturbance events (White et al. 2017). Photosynthetically active vegetation shows a higher reflectance in the near-infrared region and a lower reflectance in the shortwave infrared regions (Asner 1998) compared to non-photosynthetic and unhealthy vegetation, making it an appropriate candidate for the monitoring of forest growth processes, which involves changes in the amount of photosynthetically active vegetation through the stages of development of a stand and in function of the mortality rates. Indices derived from the tasselled cap transformation (TCT, Crist and Cicone 1984) combine the information contained in six Landsat bands. TCT derived-indices, most notably the tasselled cap wetness (TCW) and tasselled cap angle (TCA), have been associated to the density of the forest cover and have been successfully used to measure subtle forest change and to retrospectively estimate forest structural attributes (Matasci et al. 2018; Zald et al. 2016), making them relevant as tools to monitor growth even in the absence of disturbances. The normalized difference vegetation index (NDVI), relying on the NIR and red Landsat bands, is a well-known indicator of the amount of photosynthetically active vegetation, which is strongly absorptive in the red region of the spectrum (Tucker 1979). Although the NDVI is subject to saturation and is sensitive to the presence of broadleaved vegetation in boreal environments (Fiore et al. 2020; Sulla-Menashe et al. 2018), it has been used in several broad-scale studies on the effect of climate change on the growth of boreal forests (Beck and Goetz 2011; Girardin et al. 2016a) and was included in the current study to assess its performance for measuring the net basal area growth in this ecosystem.

Two categories of predictors were derived from the time series. The first category comprises the value of the VIs on the year of the first field measurement, hereafter called initial value. The second category represents the slope of the VIs over the interval between measurements and we used the Theil Sen slope estimator (Sen 1968; Theil 1950) as it has been shown to be robust against outliers and noise and has been used previously in the analysis of time series of satellite images (Bolton et al. 2020; Czerwinski et al. 2014; Rogers et al. 2018).

Modelling of the net basal area growth rate

We relied on a model selection procedure based on the second-order Akaike information criterion (AICc) to identify the best model and associated predictors from a set of candidates using the AICcmodavg package (Mazerolle 2020) in the R programming environment. Candidate models comprised one to three of the Landsat-derived predictors (Table 2), avoiding the inclusion of highly correlated variables (Pearson's $R \geq 0.8$). In the current study, model predictions were generated on a subset of the area where the training data were collected (i.e. geographic interpolation). To ensure the representativeness of the training data set, plot selection needs to be based on a form of random selection of the observations, in which all available observations had a greater than zero chance of being selected (Hastie et al. 2009; Olofsson et al. 2014; Stehman 2001). Such an approach avoids restricting the predictor space for model training, which may occur when using methods based on spatial independence constraints (Roberts et al. 2017).

We used a stratified random sampling approach based on the net growth rate measured at each plot to partition the data into training and validation data sets comprising two-thirds (120) and one-third (60) of the observations, respectively. This approach limits extrapolation when generating model predictions by ensuring a similar range of growth rates in the two data sets (Olofsson et al. 2014; Roberts et al. 2017). We then used ordinary least square (OLS) regression to train the model on the training data set. For each candidate model, assumptions were verified graphically, through the Shapiro–Wilk normality test and Verbyla's test for heteroscedasticity (Shapiro and Wilk 1965; Verbyla 1993). We used Moran's I (Moran 1950) to test for spatial autocorrelation in models residuals. We then assessed the accuracy of the best-ranked model on the validation data set.

The presence of spatial dependence in the predictor space can lead to an overestimation of model performance when using a conventional validation approach (Roberts et al. 2017). We therefore conducted an additional model performance assessment using k-fold spatial cross-validation. To conduct this step, we first tested for spatial dependence in the predictor space, using package BlockCV in the R programming environment (Valavi et al. 2018). We determined the range of spatial autocorrelation in each of the three predictors included in the best-ranked model identified after the model-selection process. The size of the spatial blocks was set as the largest range of autocorrelation amongst all predictors raster layers (i.e. TCW slope, 6000 m). We then conducted a 5-fold spatial cross-validation repeated a hundred times in order to compare model performance with the first modelling process.

LiDAR-derived information on forest structure, composition, and site characteristics

Wall-to-wall information on forest structural attributes and site moisture was obtained from an aerial single-photon LiDAR (SPL) acquisition conducted in 2018 that only encompassed the RMF. Attributes derived from the SPL directly (at a 20-m resolution) included height, canopy cover, and the rumple index (Queinnec et al. 2022b). Height was the 95th percentile of SPL return heights,

whereas canopy cover was the percentage of SPL returns above 2 m. The rumple index is the ratio of the canopy surface area on the ground surface area and is indicative of the canopy structural complexity (Kane *et al.* 2008). Area-based predictions of stem density and quadratic mean DBH were also generated at a 20-m spatial resolution using a network of temporary sample plots measured in 2019 and the SPL data (Queinnec *et al.* 2022b). To get a general indication of site moisture, the topographic wetness index (TWI, Beven and Kirkby 1979), was calculated from the 2018 SPL DEM at a 1-m resolution and averaged over the 20-m footprint of the other layers' cells. Finally, information on species composition was extracted from a species composition layer generated from the 2018 SPL data in combination with Sentinel-2 satellite imagery, indicating the dominant species in each 20-m pixel (Queinnec *et al.* 2022a).

Analysis of growth trends

The developed net basal area growth rate model was then applied over treed areas within the RMF management area. To delineate the area of model application, we used the aforementioned canopy cover and species composition layers to identify stands with similar attributes. The limited availability of LiDAR data, which was solely collected over the RMF, as well as the time gap between LiDAR acquisition and the most recent plot measurements, did not allow for the use of the LiDAR-derived attributes of the training plots for defining the model application area. Instead, we used the 20-m-resolution canopy cover layer derived from the SPL data to mask non-forested pixels, as well as areas with <50% canopy cover. A 50% canopy cover threshold was chosen to focus on stands developing as closed canopy forests, which are primarily targeted for forest management and harvest practices and to ensure the exclusion of treed bogs, frequent in the study area. We then used the species composition layer to remove areas that were dominated by species other than black spruce or jack pine. Stands that were harvested or severely disturbed between 1984 and 2021 were also excluded, using both information from the Ontario Provincial Forest Resources Inventory layer (FRI, Bilyk *et al.* 2021) and the stand-replacing disturbance history generated using the composite-to-change (C2C) approach (Hermosilla *et al.* 2016). This resulted in the exclusion of four of the training plots from the model application area, three of which were excluded because a stand-replacing disturbance had occurred between the time of the last measurement and the LiDAR acquisition.

Growth trends over the entire forest management unit

The model was applied to a 10-year moving window of BAP composites, which corresponds to the median interval between the field measurements of the plots included in the model development. This resulted in a predicted growth rate for 26 consecutive 10-year windows. Predictions were averaged to obtain the predicted growth rate over the entire study area from 1984 to 2018. We then examined the range and variability of the predicted growth rate over the study area and analyzed its evolution through time. In an additional step, we investigated the predictor values across the model application area to determine the level of extrapolation by the model. To do so, we computed the 5th, 50th, and 95th percentile, as well as the minimum and maximum value of each predictor for all of the 26 moving windows for which growth predictions were generated.

Data from the PSPs located within the RMF was used to corroborate the model predicted trends in net growth rate over the study period. We identified 64 plots, measured at least three times between 1992 and 2019, allowing the calculation of the plot-level net annual basal area growth rate on a minimum of two consecutive intervals for each plot. This criterion resulted in a different sample of plots compared to the one used in model development and validation, since plots that were measured only twice had to be rejected. Only plots in which jack pine and black spruce were the dominant species, and in which no stand replacing disturbances occurred from 1984 to 2019 were selected. The time span between the first and last field measurement ranged from 8 to 18 years during which the plots were visited either three or four times. For each interval between field visits, the plot-level net annual basal area growth rate was calculated. Then, for each plot, the change in net growth rate was calculated as the difference in net growth rates between two consecutive intervals. This step resulted in positive net growth rate change values for plots in which the net growth rate increased over time, and negative values when the net growth rate decreased in the most recent interval. The growth rate change values were then averaged at the plot level, before calculating the average growth rate change for the 64 plots. The growth rate trends derived from these data were then compared to the growth rate trends derived from the model.

Growth trends in relation to forest structure and composition

To examine differences in growth trends in relation to forest composition and structure, we grouped all pixels into a predetermined number of eight structurally distinct forest type exemplars based on the information from the SPL-derived forest attribute and species composition layers, using a *k*-means clustering approach (Hartigan *et al.* 1979). Instead of including all structural and compositional attributes in the clustering process, we first reduced the dimensionality of the data set by applying a principal component analysis (PCA), a well-established multivariate data reduction technique that allows summarizing several inter-correlated variables into a smaller number of uncorrelated variables, referred to as principal components (Abdi and Williams 2010). Using PCA before applying *k*-means clustering is an effective approach that has the advantage of minimizing the sensitivity of *k*-means clustering to the initial positions of the cluster centres (Celik 2009; Dash *et al.* 2010). The stem density, quadratic mean DBH (hereafter referred to as DBH), height, canopy cover, and value of the rumple index as well as the species dominance were all used for the PCA. The first three principal components respectively explained 45.0%, 28.3%, and 17.7% of the variance. The *k*-means algorithm was applied on the first three PCs since it captured a large percentage (i.e. 91.0%) of the variance.

For each of the resulting forest type exemplars, we extracted a 10 × 50 m profile from the 2018 SPL point cloud and summarized the average structural attributes to visualize differences between forest types. Using the forest attribute layer, areas corresponding to the average values (±5%) of the five structural attributes of each forest-type exemplars were located. We extracted the LiDAR point cloud over a 3 × 3, 20-m cells window at the locations that matched most closely to the desired structural attributes. The two-dimensional profile for each exemplar was then extracted after ensuring the forest cover was homogeneous within the point cloud. The evolution of the predicted growth through time was then plotted by extracting, for all pixels in each forest-type exemplar, the model-predicted growth rate and associated standard deviations for the 26 moving windows. Two descriptive statistics were calculated from the predicted growth time series to facilitate comparison between forest types: the average growth rate over the study period and the evolution of the growth rate through

Table 3. Ranking of the candidate models for the prediction of the net growth rate.

Model ID	Model name	AICc	Δi	Mk	Wt_i
10	**TCW slope + initial TCW value + initial NBR value**	**13.25**	**0.00**	**1.00**	**1.00**
11	NBR slope + initial TCW value + initial NBR value	28.69	15.45	0.00	0.00
8	TCW slope + initial NBR value + initial TCA value	55.28	42.03	0.00	0.00
6	TCW slope + initial NBR value	58.69	45.44	0.00	0.00
1	TCW slope	83.43	70.18	0.00	0.00
4	TCW slope + initial TCW value	84.46	71.21	0.00	0.00
9	NBR slope + initial NBR value + initial TCA value	86.26	73.02	0.00	0.00
5	NBR slope + initial NBR value	92.28	79.04	0.00	0.00
7	NBR slope + initial TCW value	106.27	93.03	0.00	0.00
2	NBR slope	110.25	97.00	0.00	0.00
12	Intercept only	123.38	110.13	0.00	0.00
3	NDVI slope	123.55	110.30	0.00	0.00

AICc is the Akaike information criterion, corrected for small sample sizes, with deltaAICc (Δi), model likelihood (Mk), and AICc weight (Wt_i). The best-performing model is indicated in bold characters.

time, hereafter referred to as the growth trend. The average predicted growth was calculated from all the pixels included in each exemplar and corresponds to the average of the predicted growth for all the 26 moving windows. Analysis of variance and multiple comparisons with the Tukey honestly significant difference (HSD) test were conducted to verify if the average growth rate was significantly different amongst the forest-type exemplars. The growth trend corresponds to the linear slope of the predicted growth values calculated over the 26 consecutive moving windows. The significance of the trend was assessed using the *t*-test statistic and associated *P*-value of the OLS regression model built from the average predicted growth rate time series of each forest-type exemplar. The location of the eight forest-type exemplars was then mapped to allow relating their unique characteristics to the spatial variations in the predicted growth over time. We then examined the average predicted growth and its slope throughout the study period in relation to the unique structural characteristics associated with each exemplar, taking into account the available knowledge on the structural development of boreal stands in this region. To allow for better visualization of the spatial distribution of the forest type exemplars within the study area, we imposed a 500-m tessellation over the initial 20-m cells in order to display the most frequently occurring structural exemplar within each 500-m cell.

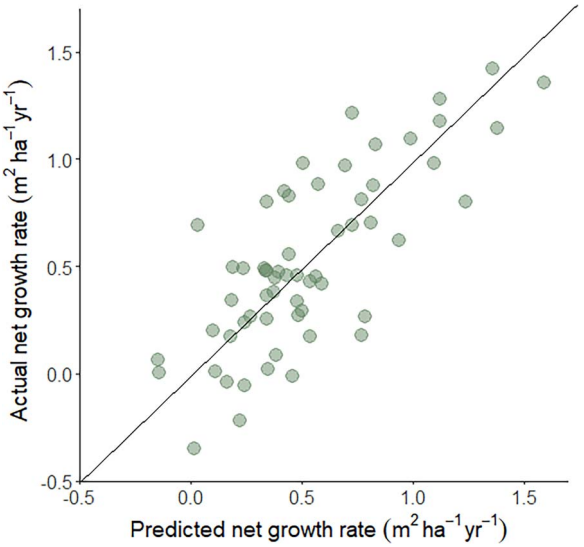

Figure 2. Actual vs predicted net growth rate (m^2 ha^{-1} yr^{-1}) of the PSPs included in the validation data set.

Results

Modelling of the net basal area growth rate

The best-performing model of net basal area growth rate, identified after the model-selection procedure conducted on the training data set ($n = 120$), included the slope of the TCW index and the initial value of both the TCW and NBR indices as predictors (Table 3). The slope of the TCW was the single predictor most strongly correlated to the net growth rate. The first-ranked model clearly stood out from the other candidates, with a model likelihood of 1 and a marked difference in AICc with the second-ranked. The spatial autocorrelation in the model residuals was not statistically significant (Moran's $I = 0.042$, *P*-value = .12), therefore we did not integrate a spatial autocorrelation structure in the OLS model. The range of growth rates and predictor values was similar between the training and validation data sets (Table 4).

The final model had an $R^2 = 0.61$ ($P < .01$, RMSE = 0.23 m^2ha^{-1} yr^{-1}) with an $R^2 = 0.58$ ($P < .01$, RMSE = 0.25 m^2ha^{-1} yr^{-1}) on the validation data ($n = 60$, Fig. 2). The R^2 and RMSE (0.61, 25.20 m^2ha^{-1} yr^{-1}) obtained from the *k*-fold spatial cross-validation were similar. The median overall predicted growth rate for the PSPs included in the validation data set was 0.46 m^2ha^{-1} yr^{-1} (standard deviation = 0.27 m^2 ha^{-1} yr^{-1}) compared to 0.47 $m^2ha^{-1}yr^{-1}$ (0.32 m^2ha^{-1} yr^{-1}) calculated from the PSP data.

Figure 3 shows the effects of the predictors included in the best-ranked model. An increase in the slope of the TCW led to an increase in the predicted net growth rate. A lower initial TCW value resulted in a higher predicted growth than for stands with a higher TCW initial value. The opposite relationship can be observed for NBR, for which a low initial value results in a lower predicted growth. The greatest predicted net growth occurs for pixels showing a highly positive TCW slope, a low initial TCW value, and a high initial NBR value.

Analysis of growth trends

Growth rate from 1984 to 2018 over the entire study area

The application of the model over a total area of 185 939 ha revealed temporal and spatial variability in the predicted growth rates. Between 1984 and 2018, the median predicted net growth rate was 0.76 m^2ha^{-1} yr^{-1}, with a standard deviation of

Table 4. Values of the predictor and response variables from plots included in the training and validation data sets as well as across the entire model application area, considering all 26 moving windows.

	TCW slope	Initial TCW value	Initial NBR value	Annual net growth rate (m^2 ha^{-1} yr^{-1})
Training plots				
5th percentile	−20.17	−688.31	0.54	−0.03
Median	−1.97	−402.28	0.65	0.47
95th percentile	30.30	−263.85	0.73	1.19
Validation plots				
5th percentile	−19.08	−710.38	0.52	0.10
Median	−1.83	−428.98	0.65	0.47
95th percentile	20.41	−244.29	0.74	1.06
Model application area				
5th percentile	−14.00	−766.72	0.56	0.23
Median	3.18	−406.25	0.67	0.70
95th percentile	31.10	−212.99	0.75	1.32

The annual net growth rates reported for training and validation plots are observed growth rates, whilst growth rates reported for the model application area are predicted values.

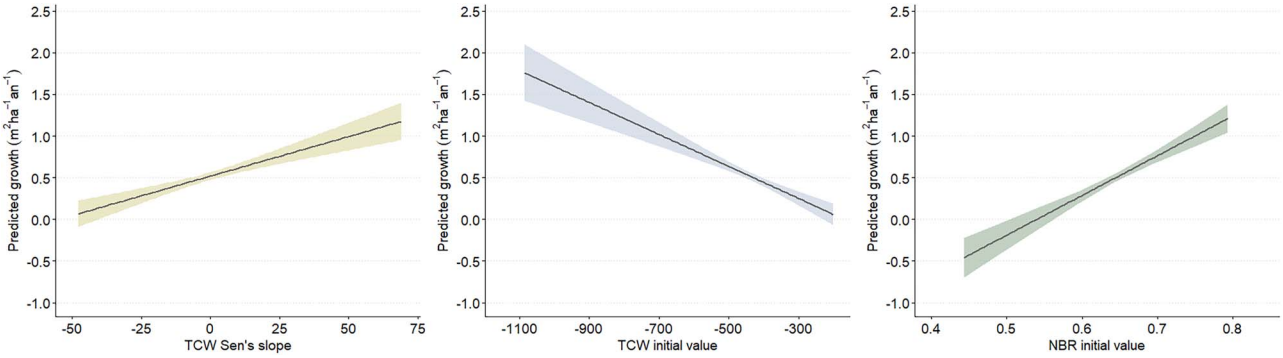

Figure 3. Model predictions and unconditional 95% confidence intervals for the best-fit model parameters.

0.09 m^2ha^{-1} yr^{-1}. There was a considerable range in predictions with a 5th percentile at 0.35 m^2ha^{-1} yr^{-1} and a 95th percentile at 1.31 m^2ha^{-1} yr^{-1} (Figs 4a and 6a). This was greater than the median net growth rate measured in the training and validation PSPs (0.47 m^2ha^{-1} yr^{-1}. standard deviation = 0.38 m^2ha^{-1} yr^{-1}), but within the range of the growth rates measured in the PSPs, with minimum and maximum values of −0.39 and 1.90 m^2ha^{-1} yr^{-1}, respectively (Table 4). The median predicted growth rates were highly variable across the study site, as shown in Figure 6.

Decomposing the time series in 10-year moving windows allowed for visualizing the evolution of the predicted growth rate over time (Figs 4b and 6b). In most of the model application area, predictions were made within the range of predictor values extracted over the plots included in the training data set. The range of predictor values across the entire model application area are presented in Table 4. Since the growth rate statistics presented in Table 4 are derived from predictions across all 26 moving windows, they differ from the values averaged for the period 1984–2018.

Whilst the median net growth rate reached 0.92 m^2ha^{-1} yr^{-1} for the 1984–93 period, it was considerably lower at the end of the study period, with a median predicted net growth of only 0.61 m^2ha^{-1} yr^{-1} for the 2009–18 period, the lowest observed of all 26 moving windows. The highest median predicted growth was in the 1985–94 period (0.93 m^2ha^{-1} yr^{-1}). Between 1984 and 2018, the predicted growth averaged across the entire study site showed a significant negative linear trend ($P = .017$), decreasing by an average of 0.007 m^2ha^{-1} yr^{-1} from one moving window to the next.

The net growth rate also tended to decrease over time in the PSPs, with an average change of −0.048 m^2ha^{-1} yr^{-1} (standard deviation = 0.59 m^2ha^{-1} yr^{-1}) between consecutive measurement intervals, although the growth rate increased over time in 41% of the plots (Fig. 5). The median annual net growth rate observed in PSPs measured at least three times between 1992 and 2019 was 0.43 m^2ha^{-1} yr^{-1}. This is slightly lower than the median growth rate measured in the selection of PSPs used for model development and validation (0.47 m^2ha^{-1} yr^{-1}), which also included plots measured only twice during the study period, but excluded plots that were located < 80 m away from roads, waterbodies, and stand boundaries.

Growth trends in relation to forest structure and composition

The eight forest-type exemplars identified after the clustering procedure were characterized by distinct structural and compositional attributes, described in Fig. 7 and Table 5. These attributes are representative of the various development stages expected in boreal forests of this region (Oliver and Larson 1996). The average predicted growth rate calculated over the entire study period was significantly different between all exemplars ($P < .001$) and ranged from 0.60 to 0.90 m^2ha^{-1} yr^{-1} (Table 6).

Exemplars 1, 2, and 4 were characterized by high mean growth rates over the entire study period, but the most pronounced and statistically significant negative growth trends amongst all exemplars (Table 5). Exemplar 1, dominated by black spruce, was the fastest growing and also the most common, accounting for

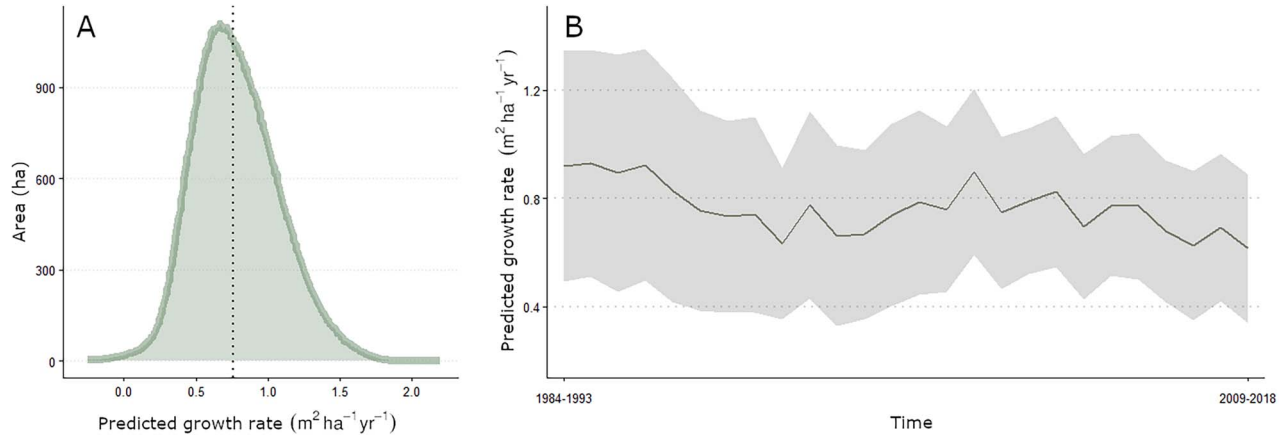

Figure 4. (a) Distribution of the predicted growth rate ($m^2 ha^{-1}\ yr^{-1}$) over the study area from 1984 to 2018 obtained by averaging the predictions computed on 26 10-year moving windows. Vertical dotted line indicates the median. (b) Evolution of the average predicted growth from 1984 to 2018 for the 26 10-year moving windows. The shaded region indicates the standard deviation.

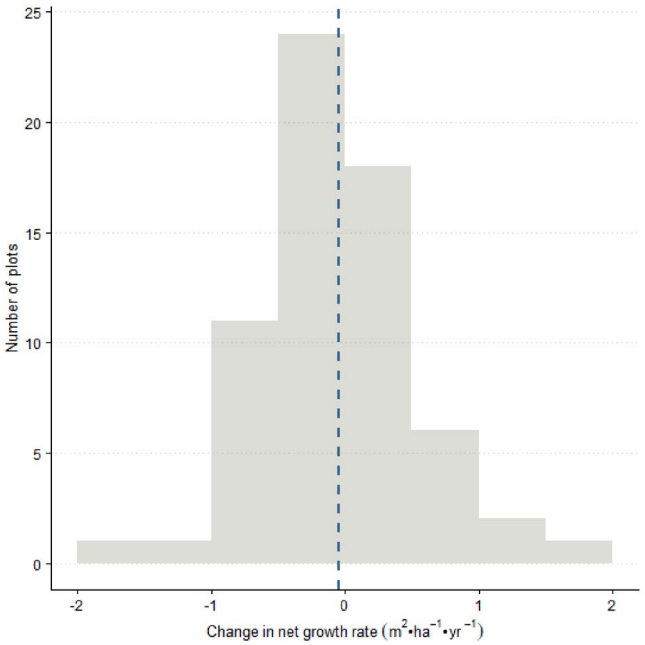

Figure 5. Distribution of the plot-averaged changes in net growth rate ($m^2 ha^{-1}\ yr^{-1}$) measured in the permanent sample plots located within the RMF between 1992 and 2019. Dotted line indicates the average.

21.4% (39 715.6 ha) of the area included in the analysis. Conversely, Exemplar 4, dominated by jack pine, was the least spatially extensive exemplar in the study area, accounting for only 9054.5 ha (4.9%). These two exemplars were characterized by the highest stem density values and high canopy cover, but low canopy complexity, as indicated by their low rumple index values. Representative of stands dominated by black spruce, Exemplar 2 accounted for 13.0% (25 151.5 ha) of the study area. This exemplar was characterized by very low height and DBH, average density and canopy cover values, and the second-highest TWI value. Accounting for almost 40% of the study area, Exemplars 1, 2, and 4 were mainly concentrated in the western and south-eastern regions of the study area (Fig. 8). Their rapid growth at the beginning of the study period is followed by a gradual decrease, which is readily visible in Fig. 7.

Exemplars 3, 5, and 8 also showed significantly negative growth trends throughout the study period, although less pronounced than those of Exemplars 1, 2, and 4 (Table 5, Fig. 7). These exemplars had substantial differences in their mean growth rate during the study period. Dominated by black spruce, Exemplars 3 and 5 accounted for 14.7% (27 280.4 ha) and 15.4% (28 679.4 ha) of the area included in the study, respectively, and were relatively evenly distributed within the study area (Fig. 8). They had average values of stem density, DBH, height, and rumple index, but a relatively high canopy cover, with Exemplar 3 being the one with the highest values for all structural attributes amongst both. Exemplar 8 was dominated by jack pine and occupied only 5.9% (11 003.5 ha) of the study area and was mostly concentrated in the eastern part of the study area (Fig. 8). Exemplar 8 had the lowest average growth rate over the study period amongst all exemplars and had high rumple index, height, and DBH values, but a low stem density and canopy cover. The structural attributes of Exemplar 6 were similar to that of Exemplar 8, but Exemplar 6 was dominated by black spruce. Exemplar 6 occupied 11.2% (20 897.1 ha) of the area included in the analysis, showed a higher predicted growth than Exemplar 8 and did not show either a positive or negative trend in growth over the study period. Finally, Exemplar 7 was dominated by black spruce and accounted for 13.5% (25 157.0 ha) of the study area. This exemplar had the second-lowest average predicted growth, but did not show a significant trend in growth between 1984 and 2018. Exemplar 7 was characterized by a low stem density and the lowest canopy coverage, DBH, and height values, but showed a high rumple index value. This exemplar was concentrated on the northernmost part of the RMF (Fig. 8) making it easily noticeable in Fig. 7, since it displayed a slow growth rate throughout the entire 1984–2018 period.

Discussion

In this study, we demonstrate how Landsat time series can be used to generate spatially explicit information on coniferous-dominated boreal forest net growth rate (annual basal area increment) in the absence of stand-replacing disturbances. Furthermore, airborne LiDAR data were used to indicate how predictions of growth rates are representative of differences in stand development stages, species composition, and structural attributes.

The field-calibrated and validated model provides wall-to-wall predictions of average annual net basal area growth rate over the

Table 5. Average structural attributes, predicted growth rates, and slopes of the growth trend for the eight forest-type exemplars.

Forest-type exemplar	Proportion of the study area (%)	Dominant species	DBH (cm)	Density (stems · ha^{-1})	Height (m)	Canopy coverage (%)	Rumple index	TWI	Mean predicted growth rate (m^2 ha^{-1} yr^{-1})	Trend in predicted growth rate	Median FRI age in 2018
1	21.4	Black spruce	13.9 (0.9)	1976 (197)	14.0 (1.7)	91.9 (4.4)	2.84	8.9 (4.3)	0.90	−0.011***	83
2	13.0	Black spruce	12.9 (0.9)	1393 (197)	11.7 (1.1)	76.6 (7.7)	2.99	10.4 (4.5)	0.83	−0.010***	88
3	14.7	Black spruce	17.6 (0.9)	1620 (168)	18.1 (1.4)	90.8 (4.4)	3.60	8.0 (3.9)	0.79	−0.005**	93
4	4.9	Jack pine	15.9 (1.8)	1886 (373)	16.9 (2.2)	84.8 (7.5)	2.69	8.2 (4.0)	0.75	−0.022***	63
5	15.4	Black spruce	14.9 (0.8)	1468 (236)	15.0 (1.1)	82.1 (5.4)	3.61	9.1 (4.3)	0.73	−0.006*	93
6	11.2	Black spruce	18.9 (1.2)	1126 (183)	18.7 (1.8)	77.5 (8.8)	4.55	9.0 (4.3)	0.67	−0.002	98
7	13.5	Black spruce	15.4 (1.2)	1062 (188)	14.4 (1.4)	65.4 (7.5)	3.90	10.5 (4.5)	0.66	−0.002	98
8	5.9	Jack pine	20.3 (1.8)	1160 (237)	21.3 (2.2)	78.6 (9.7)	4.52	7.5 (3.7)	0.60	−0.006**	93

Values in parentheses indicate standard deviation. Asterisks indicate the level of significance of the linear slope of the growth time series calculated over the 26 10-year moving windows (*** 0.001, ** 0.01, * 0.05).

past 36 years for undisturbed forests within a large forest management unit, which is critical information for silvicultural decision-making (Forrester 2019). The developed net growth rate predictive model explained a substantial proportion of the variance in net growth rates measured from field data (58%, Fig. 2).

Amongst the tested predictors, the Theil Sen slope of the TCW is the best linked to net growth rate. The TCW is known to be correlated to various forest structural attributes such as average stand DBH, height, crown diameter, density, and basal area, making it a reliable indicator of stand development stages in closed canopy forests (Cohen *et al.* 1995; Cohen and Spies 1992; Hansen *et al.* 2001). Landsat-derived TCW has been successfully used to detect forest growth and decline (Czerwinski *et al.* 2014), and to map forest structural attributes and aboveground biomass (Bolton *et al.* 2020; Matasci *et al.* 2018; Zald *et al.* 2016). These results confirm that spectral indices utilizing shortwave-infrared reflectance are the most appropriate Landsat-derived vegetation indices to monitor forest structural development through time. The poor correlation of NDVI with net growth brings additional evidence of the limited capacity of this index to capture processes of forest growth and decline in high canopy cover forest (Fiore *et al.* 2020; Sulla-Menashe *et al.* 2018).

The initial condition of the forest was important in predicting subsequent growth. The first-ranked model included the initial value of both the TCW and the NBR. Indicative of earlier stages of stand development, low initial TCW values are associated with higher growth rates in the following period. This is consistent with the typical evolution of growth rates in boreal forests, being faster at early stages of development and gradually slowing down once canopy closure is reached (Chen and Popadiouk 2002; Harper *et al.* 2005). Interestingly, lower initial NBR values are linked to subsequent slower growth. Low NBR values are associated with a higher proportion of non-photosynthetically active vegetation or more exposed soil when compared to areas with higher NBR values (Asner 1998; Clevers 1988). In undisturbed forests, a low initial NBR may therefore suggest a sparse, less productive site, or stands that have previously experienced stress or mortality and are more likely to grow slowly in the future.

Changes in growth rate over the study period

The application of the predictive model on 10-year moving windows allowed for the visualization of the spatial and temporal variability in growth rates within the study site between 1984 and 2018 (Figs 4b and 6b). Figure 6 highlights this variability; while some areas of the RMF showed a sustained growth rate across all moving windows, a gradual decline in the predicted growth rate is observed in some regions. The generalized growth decline revealed by model predictions during the investigated period (Fig. 4b), corroborated by the decline in growth rates observed in the permanent sample plots located within the study site (Fig. 5) is mainly attributable to an age-related decrease in growth rates. The analysis of growth trends was conducted exclusively on stands that were established before 1984, creating a bias due to the progressive reduction of the growth rate associated with stand age (Chen *et al.* 2002). The high median growth rate observed in the first 10-year moving window (i.e. 1984–93) is related to the presence of young stands, regenerating consecutively to clear-cuts conducted from 1973 to 1983 on a total area of 8876 ha. The median growth rate predicted over this area went from 1.58 m^2 ha^{-1} yr^{-1} in the 1984–93 period, to only 0.73 m^2 ha^{-1} yr^{-1} in the 2009–18 period.

Fluctuations in the predicted growth rate within the study period may, however, be attributable to other factors, such as a growth response to environmental stressors. The predicted growth rate showed a substantial decrease in 1988–97 that lasted until the 1997–2006 period (Fig. 4b). In June, July, and August 2001, abnormally low amounts of precipitation accompanied by higher than normal temperatures resulted in 110 306 ha of visible drought damage in the Timmins District in Ontario, where our study site is located (MNRF 2001). Examination of the values of the standardized precipitation evapotranspiration index (SPEI, Vicente-Serrano *et al.* 2010) during the study period also revealed abnormally low values in 1997, 2005, and 2011, which could have also impacted forest growth.

A widespread increase in mortality rates was observed in Canadian boreal forests between 1963 and 2008. Jack pine and black spruce, the most abundant species in our study area, both showed a significant increase in mortality rates during this period (Peng *et al.* 2011). The mortality rates of these species were significantly and positively correlated to temperature, which increased continuously at our study site during the same period. Mean annual temperatures over the RMF, modelled using BioSim (Version 11; Régnière *et al.* 2017) followed a significantly increasing trend ($P = .01$) between 1970 and 2018 with an average annual increase of 0.02°C. Marchand *et al.* (2019) also detected negative growth trends in black spruce and jack pine tree rings at several locations in the neighbouring province of Quebec between 1970 and 2005. The most widespread explanation for these growth declines in the boreal forest is related to an increase in temperatures that would cause some boreal stands to shift from temperature- to moisture-limited growth (Chagnon *et al.* 2022; D'Orangeville *et al.* 2018; Girardin *et al.* 2016b; Peng *et al.* 2011). Although small to

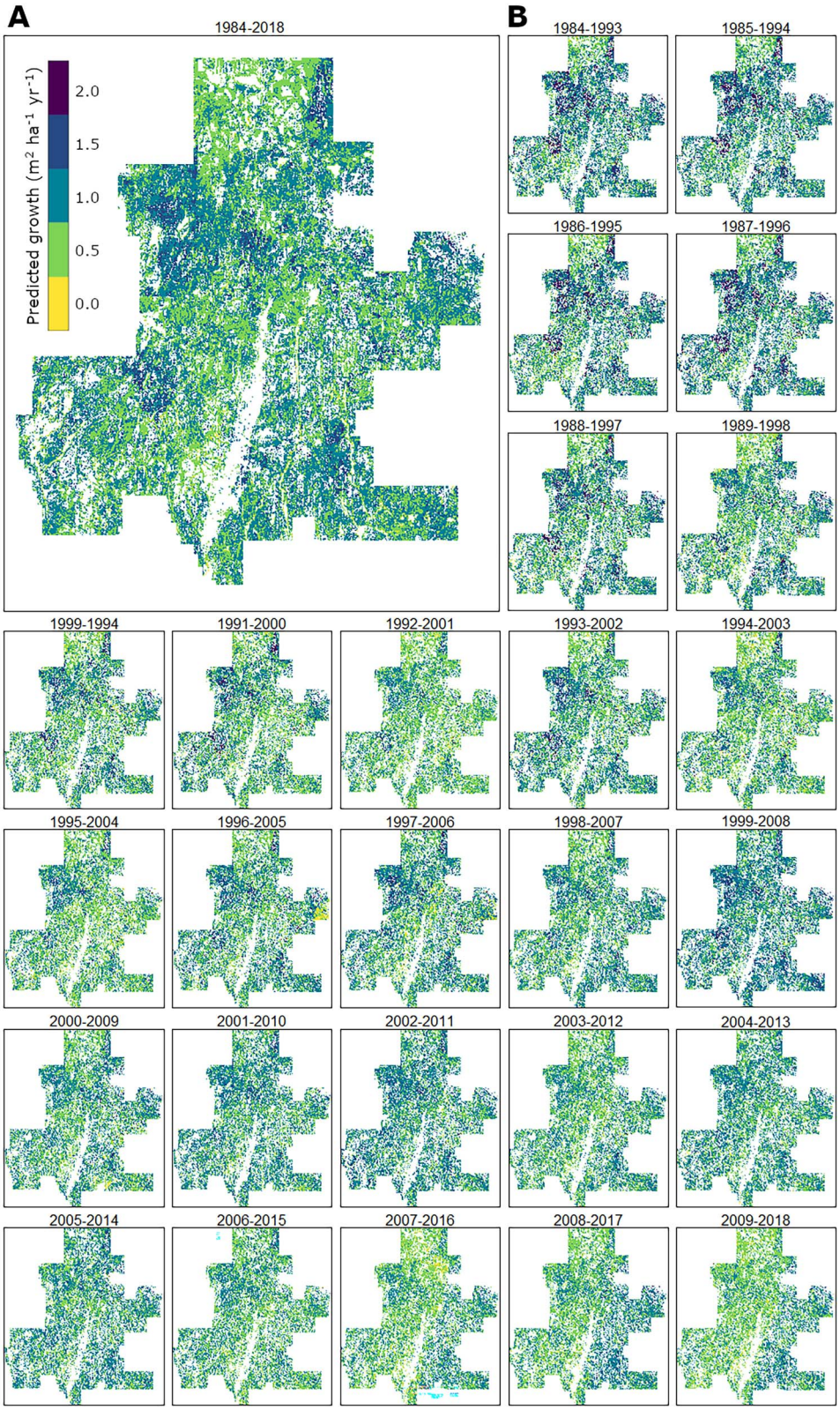

Figure 6. (a) Predicted growth rate ($m^2 ha^{-1} yr^{-1}$) over the study area from 1984 to 2018 obtained by averaging predictions computed on 26 10-year moving windows. (b) Predicted growth rate ($m^2 ha^{-1} yr^{-1}$) over the study area from 1984 to 2018 decomposed in 26 10-year moving windows.

moderate increases in temperature are expected to have positive effects on the growth of boreal species, higher increases in temperature that are not accompanied by higher amounts of precipitation can have detrimental effects, especially in sites were topography or a coarser deposit makes the water availability low (Marchand *et al.* 2019). Soil water availability was found to be significantly correlated to the growth of black spruce forests in many regions, and is expected to become an increasingly

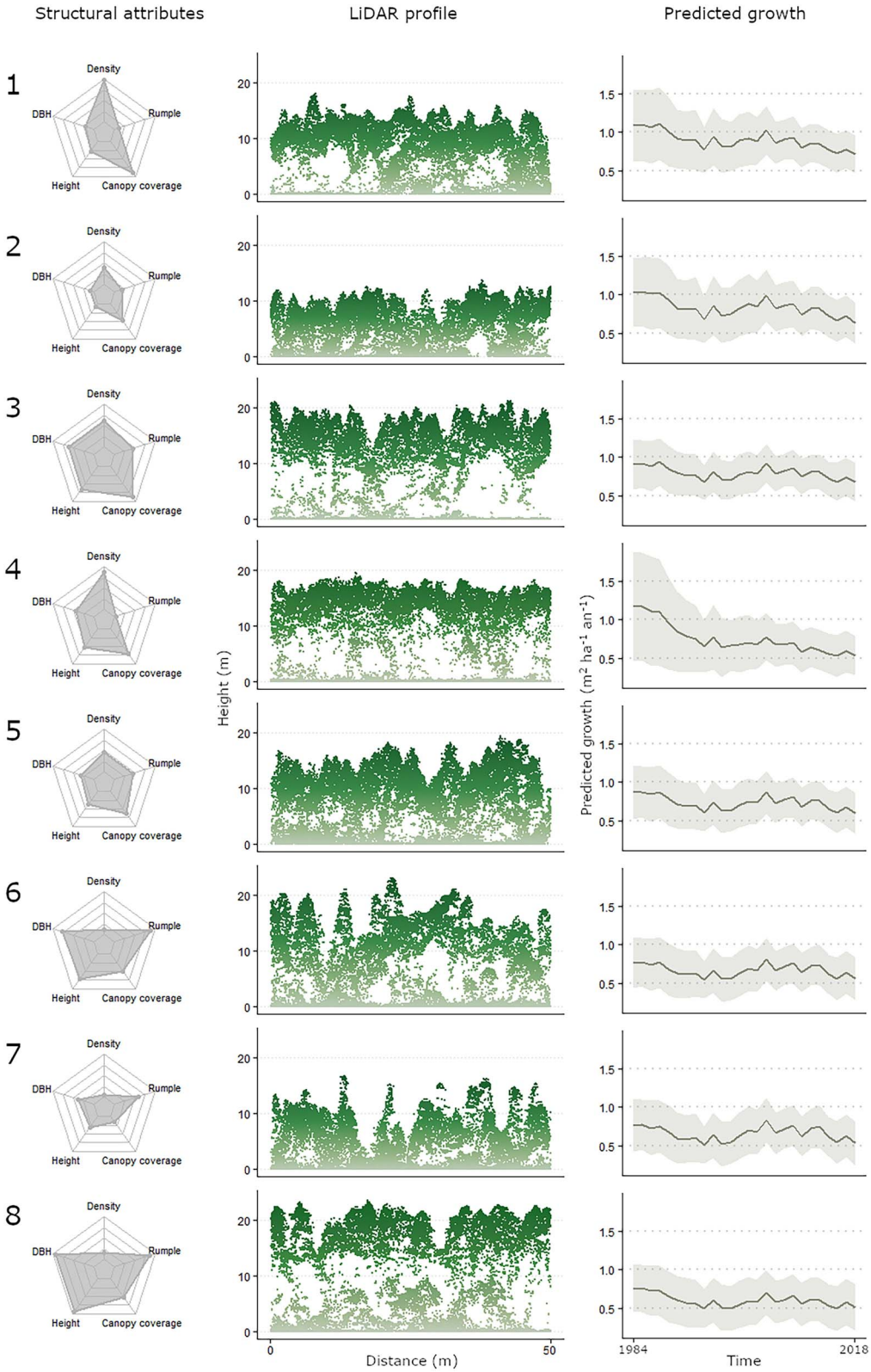

Figure 7. Characteristics of the eight forest-type exemplars. The first column shows the main structural parameters, extracted from the forest attributes layer generated using SPL data. The second column shows the normalized SPL profiles illustrating the typical forest structure associated with each of the forest-type exemplars. Each profile has a width of 10 m and a length of 50 m. The third column shows the model-predicted growth of each forest-type exemplar from 1984 to 2018, calculated over 26 10-year moving windows. The exemplars are presented in decreasing order of average predicted growth during the study period. The number on the left indicated the cluster number used in the text.

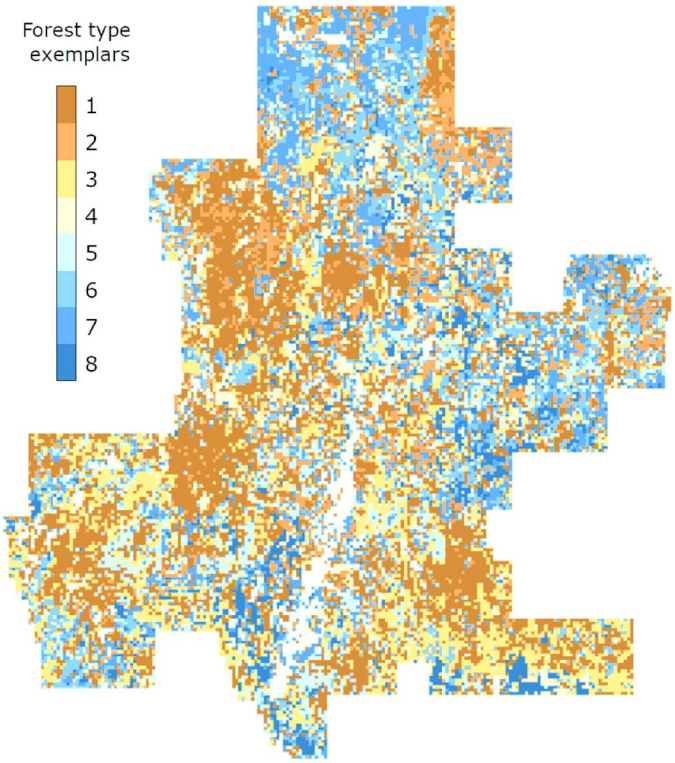

Figure 8. Location of the forest-type exemplars within the study site. For visualization, the 20-m pixels were aggregated into 500-m pixels showing the dominant forest-type exemplar.

important driver of productivity in the boreal zone (Chagnon *et al.* 2022; Girardin *et al.* 2016b; Peng *et al.* 2011). On the drier sites, jack pines would also be more likely to die prematurely, because of the species' small physiological margin of safety from hydraulic failure during drought (Mamet *et al.* 2015). The vulnerability of this species to pathogens has also been found to be higher on sites with low available water-holding capacities, by influencing carbon mobilization, allocation, and utilization for defence responses (Hussain *et al.* 2020).

Growth trends in relation to forest structural attributes and composition

The model-predicted growth of the identified forest-type exemplars is consistent with previous research on the structural development of boreal stands in the same region (Harper *et al.* 2005; Smirnova *et al.* 2008). The statistically significant decreasing slope of the predicted growth for Exemplars 1, 2, and 4 suggest that these stands are at an early stage of development. This is supported by the rumple index which is the lowest amongst all exemplars, indicating relatively homogeneous canopy surfaces and low structural complexity (Kane *et al.* 2010). The high stem density and canopy cover of Exemplars 1 and 4 are typical of the transition from the stand initiation stage to the stem exclusion stage, where trees that established successfully and grew rapidly in open conditions are now occupying most of the available growing space, reaching canopy closure (Harper *et al.* 2005; Oliver and Larson 1996; Smirnova *et al.* 2008). The moment at which trees start experiencing competition for light and other resources occurs faster in jack pine dominated stands than in black spruce dominated stands because of faster juvenile growth rates (Harper *et al.* 2003). The jack pine-dominated Exemplar 4 indeed shows the highest predicted growth rate during the 1984–93 period (1.17 m^2 ha^{-1} yr^{-1}), followed by the black spruce-dominated Exemplar 1 (1.09 m^2 ha^{-1} yr^{-1}). Compared to the latter, Exemplar 2, which was also dominated by black spruce, has a lower density, canopy coverage and the lowest height, typical of the stand initiation stage or to forests developing on low productivity sites (Harper *et al.* 2005; Oliver and Larson 1996). This exemplar had the second highest TWI value, indicative of hydric conditions. Development of boreal stands on organic and hydric sites occurs on a considerably longer timescale than on mesic sites and do not necessarily follow the development stages expected in managed boreal forests (Oliver and Larson 1996), since they may never reach full canopy closure and experience self-thinning due to competition (Harper *et al.* 2005). Although reliable information on stand age was not available over the entire study area, especially for older stands, data from the FRI on recent silvicultural interventions reveal that 82.4% of the area harvested from 1973 to 1983 (8876 ha) was classified either in Exemplars 1, 2, or 4, which is consistent with the observed patterns in model-predicted growth.

The structural attributes and growth patterns of Exemplars 3 and 5 suggest they have reached the stem exclusion stage (Harper *et al.* 2005; Oliver and Larson 1996). The progressive decrease in growth rates associated with these exemplars, as indicated by a significant decreasing trend in the predicted growth, was less substantial than in the case of Exemplars 1, 2, and 4. Their lower stem density values, but relatively high height, DBH, and rumple index values are indicative of stands that entered the stem exclusion stage, where trees start experiencing the consequences of competition, leading to the mortality of trees with a less favourable position in the canopy, associated with a progressive reduction in stem density and growth at the stand level (Oliver and Larson 1996). Differences in the predicted growth between these two exemplars may be attributable to differences in age or site productivity.

Exemplars 6, 7, and 8 have the lowest average predicted growth rate over the study period, consistent with their structural

attributes that are indicative of older stands. These exemplars have the highest rumple index values, indicative of complex canopy surfaces, high DBH values, and low stem density. The low stem density of Exemplars 6 and 8 are likely due to a pronounced self-thinning due to mortality from competition, environmental, or age-related factors typical of the understory reinitiation stage (Oliver and Larson 1996). Exemplar 7 is probably representative of an alternative stand development trajectory; with the highest TWI value, the lowest canopy coverage, and the third-lowest height, it possesses the characteristics of old black spruce stands located on hydric sites (Harper *et al.* 2005). On these less productive sites, stands may never reach canopy closure and are growing slowly, but continuously for a period that can last until 200–250 years of age, whilst growth reaches a peak and decreases considerably earlier on more productive sites (Harper *et al.* 2003). This is supported by a lack of a significant trend in the predicted growth of Exemplar 7 over the 26 moving windows. Conversely, Exemplar 8 showed the lowest average growth rate and a significant reduction in the predicted growth rate throughout the study period. This exemplar, characterized by the lowest TWI value, may be representative of the succession pathway of stands with high jack pine component on coarse deposits, where growth is sustained in the early development stages, but decreases more rapidly than black spruce dominated stands (Harper *et al.* 2005). Because of their shorter longevity (i.e. 70–100 years), jack pine trees will eventually disappear, leaving space for the more shade tolerant black spruce and leading to an eventual decrease in forest canopy coverage and height (Harper *et al.* 2002; Smirnova *et al.* 2008).

Implications for the management of boreal stands

The growth of boreal stands is influenced by numerous internal and external factors, such as stand age, structural attributes, and species composition, as well as site characteristics such as topography and surface deposits. For instance, a decline in growth rate is expected to occur earlier on productive sites dominated by jack pine than on less productive sites dominated by black spruce (Harper *et al.* 2003). Changes in the growth rate can also happen in response to physiological stresses, caused notably by limited water availability due to topography or the nature of surficial deposits (Johnstone *et al.* 2010; Marchand *et al.* 2019).

The availability of high-resolution, spatially explicit information on forest growth rates and the evolution of the growth rate over time offer the possibility of applying more precise and agile silviculture practices by discriminating actively growing stands from those that are stagnating or declining at the scale of a management unit. This information is crucial for efficient forest management (Forrester 2019), but can be challenging to obtain using traditional inventory approaches that provide only a partial and intermittent picture of forest growth, since ground plots are spatially and temporally constrained, i.e. limited in number and measured only periodically (Bowman *et al.* 2013; Gillis *et al.* 2005).

By combining information on forest stand structure derived from LiDAR data with growth information derived from Landsat time series, targeted silvicultural interventions could be carried out to stimulate the growth of stagnating stands, promote the resistance and resilience of vulnerable stands, or determine the best time for harvesting. Studying past growth rates and linking those with stand structure could enable the development of a library of representative growth curves for specific sites and species, thereby improving yield predictions (Boisvenue and White 2019).

Limitations and future work

The approach developed in the current study is specifically designed for monitoring of gradual changes in undisturbed forests. A substantial proportion of boreal stands in Canada however will likely experience some form of disturbances be it from natural disturbances or silvicultural treatments. The relationships between the effect of these events on stand-level growth dynamics, structural attributes, and canopy spectral reflectance are complex and highly variable depending on the disturbance agent, making model-predicted growth rates more complex in this context. To be broadly applicable to boreal forests of Canada, the approach proposed in this study could be integrated within a continuous inventory framework, in which change detection algorithms are used to detect disturbances and stand attributes are updated accordingly (e.g. Coops *et al.* 2023). Combining these approaches would enable spatial and temporal delineation of the areas and periods for which model predictions could be generated reliably. Other studies have used similar approaches to exclude disturbed areas from productivity assessments (Moan *et al.* 2023).

In the current study, growth rate predictions were generated using constant length, 10-year moving windows, which corresponds to the median interval between field measurements of the plots used for model development and validation. However, the interval between field measurements varied widely, ranging from 5 to 24 years. Despite such a large range, we could not find any patterns in the magnitude of errors in model predictions as a function of the length of the time between field measurements. Calculation of the predictions on shorter or longer intervals may, however, have produced slightly different results. The optimal window length should be investigated further and taken into account in the future development and application of such models, since related studies have concluded to the importance of this factor (Bolton *et al.* 2020).

It is likely that the drought events and the continual rise in mean temperatures observed in the study area contributed to changes in moisture regimes, which played a role in the fluctuation of forest growth rates. The number of forest-type exemplars presented in this study was determined arbitrarily and do not likely encompass all of the variability in site conditions, forest structure, composition, and associated growth patterns within the study area. The clustering method employed focused exclusively on undisturbed forests and resulted in a fixed number of classes, which could have been expanded to capture more variability in growth conditions. Each forest-type exemplar represented between 9054 and 39 715 ha of forest land and did not consider differences in site conditions or stand age, both of which are important factors in growth response to environmental conditions. Accounting for these factors could have revealed more pronounced differences between forest types. As a result, the diversity in observed growth patterns was limited, with many exemplars showing trends that were similar to that of the entire forest management unit. Additionally, most exemplars exhibited large within-class variability in predicted growth rates, likely due to differences in site conditions, as evidenced by the high standard deviation of the TWI values within each exemplar. Nonetheless, differences in the structural and compositional attributes of the exemplars were sufficient to reveal dissimilarities in the average predicted growth and growth trends throughout the study period.

Future research will focus on evaluating the model's ability to capture differences in predicted growth rates amongst sites with varying levels of sensitivity to climate stressors using climate data and field-collected soil and growth data. This capacity to retrospectively assess the spatial manifestations of climate stressors

on forest growth may also help inform the development of climate sensitive growth and yield models.

Conclusion

In the face of increasing uncertainty surrounding future growth and forest condition under changing environmental conditions, responsible and adapted forest management practices require the development of methods that enable spatially explicit monitoring of forest growth rates and their evolution over time. Our study demonstrates that a field-calibrated and -validated model, developed using Landsat time series, can predict the annual net basal area growth rate for undisturbed forests and reveal differences in growth rates that are consistent with stand development stage and species composition, as determined using airborne LiDAR and Sentinel-2 data. Linking a forest stand's structural attributes with the evolution of growth over time has the potential to address several current challenges in the forest management domain. The proposed approach could eventually be used to create baseline growth trajectories for various forest types on different site conditions that could then be integrated into a near-real-time forest inventory framework, allowing for the updating of forest attribute layers in undisturbed forests. The information generated by this approach can improve yield predictions, optimize rotation lengths, and identify target areas where silvicultural interventions aimed at maintaining or enhancing growth could be conducted.

Acknowledgements

We would like to acknowledge our collaborators from the Ministry of Natural Resources and Forestry for sharing data from the Growth and Yield and Vegetation Sampling Network databases, and give special thanks to Dave Morris, Todd Little and Muhammad Waseem Ashiq for their help. We would also like to thank Chris McDonell from GreenFirst Forest Products and Grant McCartney from Forsite Consultants for their help in accessing and assembling the data required for this study.

Conflict of interest

None declared.

Funding

The NSERC Alliance project Silva21 (NSERC ALLRP 556265-20 to A.A.); the NSERC Alexander Graham Bell Graduate Scholarships-Doctoral Program (CGS-D to A.M.B.).

Data availability

The data underlying this article were provided by the Ontario Ministry of Natural Resources and Forestry. Data will be shared on reasonable request to the corresponding author with permission of the Ontario Ministry of Natural Resources and Forestry.

References

Abdi H, Williams LJ. Principal component analysis. *Wiley Interdiscip Rev Comput Stat* 2010;**2**:433–59. https://doi.org/10.1002/wics.101.

Achim A, Moreau G, Coops NC. *et al.* The changing culture of silviculture. *Forestry* 2022;**95**:143–52. https://doi.org/10.1093/forestry/cpab047.

Asner GP. Biophysical and biochemical sources of variability in canopy reflectance. *Remote Sens Environ* 1998;**64**:234–53. https://doi.org/10.1016/S0034-4257(98)00014-5.

Baltsavias EP. Airborne laser scanning: basic relations and formulas. *ISPRS J Photogramm Remote Sens* 1999;**54**:199–214. https://doi.org/10.1016/S0924-2716(99)00015-5.

Banskota A, Kayastha N, Falkowski MJ. *et al.* Forest monitoring using Landsat time series data: a review. *Can J Remote Sens* 2014;**40**:362–84. https://doi.org/10.1080/07038992.2014.987376.

Beck PSA, Goetz SJ. Satellite observations of high northern latitude vegetation productivity changes between 1982 and 2008: ecological variability and regional differences. *Environ Res Lett* 2011;**6**:045501. https://doi.org/10.1088/1748-9326/6/4/045501.

Beven KJ, Kirkby MJ. A physically based, variable contributing area model of basin hydrology/Un modèle à base physique de zone d'appel variable de l'hydrologie du bassin versant. *Hydrol Sci J* 1979;**24**:43–69. https://doi.org/10.1080/02626667909491834.

Bilyk A, Pulkki R, Shahi C. *et al.* Development of the Ontario Forest Resources Inventory: a historical review. *Can J For Res* 2021;**51**:198–209. https://doi.org/10.1139/cjfr-2020-0234.

Boisvenue C, White JC. Information needs of next-generation forest carbon models: opportunities for remote sensing science. *Remote Sens* 2019;**11**:463. https://doi.org/10.3390/rs11040463.

Bolton DK, Tompalski P, Coops NC. *et al.* Optimizing Landsat time series length for regional mapping of LiDAR -derived forest structure. *Remote Sens Environ* 2020;**239**:111645. https://doi.org/10.1016/j.rse.2020.111645.

Bowman DMJS, Brienen RJW, Gloor E. *et al.* Detecting trends in tree growth: not so simple. *Trends Plant Sci* 2013;**18**:11–7. https://doi.org/10.1016/j.tplants.2012.08.005.

Brandt JP, Flannigan MD, Maynard DG. *et al.* An introduction to Canada's boreal zone: ecosystem processes, health, sustainability, and environmental issues. *Environ Rev* 2013;**21**:207–26. https://doi.org/10.1139/er-2013-0040.

Brecka AFJ, Shahi C, Chen HYH. Climate change impacts on boreal forest timber supply. *Forest Policy Econ* 2018;**92**:11–21. https://doi.org/10.1016/j.forpol.2018.03.010.

Celik T. Unsupervised change detection in satellite images using principal component analysis and k-means clustering. *IEEE Geosci Remote Sens Lett* 2009;**6**:772–6. https://doi.org/10.1109/LGRS.2009.2025059.

Chagnon C, Wotherspoon AR, Achim A. Deciphering the black spruce response to climate variation across eastern Canada using a meta-analysis approach. *For Ecol Manage* 2022;**520**:120375. https://doi.org/10.1016/j.foreco.2022.120375.

Chen HY, Popadiouk RV. Dynamics of North American boreal mixedwoods. *Environ Rev* 2002;**10**:137–66. https://doi.org/10.1139/a02-007.

Chen W, Chen JM, Price DT. *et al.* Effects of stand age on net primary productivity of boreal black spruce forests in Ontario, Canada. *Can J For Res* 2002;**32**:833–42. https://doi.org/10.1139/x01-165.

Clevers JGPW. The derivation of a simplified reflectance model for the estimation of leaf area index. *Remote Sens Environ* 1988;**25**:53–69. https://doi.org/10.1016/0034-4257(88)90041-7.

Cohen WB, Spies TA. Estimating structural attributes of Douglas-fir/western hemlock forest stands from Landsat and SPOT imagery. *Remote Sens Environ* 1992;**41**:1–17. https://doi.org/10.1016/0034-4257(92)90056-P.

Cohen WB, Spies TA, Fiorella M. Estimating the age and structure of forests in a multi-ownership landscape of western Oregon, U.S.A. *Int J Remote Sens* 1995;**16**:721–46. https://doi.org/10.1080/01431169508954436.

Coops NC, Tompalski P, Goodbody TR. *et al.* Framework for near real-time forest inventory using multi source remote sensing data. *Forestry* 2023;**96**:1–19. https://doi.org/10.1093/forestry/cpac015.

Crist EP. A TM tasseled cap equivalent transformation for reflectance factor data. *Remote Sens Environ* 1985;**17**:301–6. https://doi.org/10.1016/0034-4257(85)90102-6.

Crist EP, Cicone RC. A physically-based transformation of thematic mapper data—the TM tasseled cap. *IEEE Trans Geosci Remote Sens* 1984;**GE-22**:256–63. https://doi.org/10.1109/TGRS.1984.350619.

Czerwinski CJ, King DJ, Mitchell SW. Mapping forest growth and decline in a temperate mixed forest using temporal trend analysis of Landsat imagery, 1987-2010. *Remote Sens Environ* 2014;**141**:188–200. https://doi.org/10.1016/j.rse.2013.11.006.

Dash B, Mishra D, Rath A. *et al.* A hybridized K-means clustering approach for high dimensional dataset. *Int. J Eng Sci* 2010;**2**:59–66. https://doi.org/10.4314/ijest.v2i2.59139.

Dietrich R, Bell FW, Silva LCR. *et al.* Climatic sensitivity, water-use efficiency, and growth decline in boreal jack pine (*Pinus banksiana*) forests in Northern Ontario. *J Geophys Res Biogeo* 2016;**121**:2761–74. https://doi.org/10.1002/2016JG003440.

D'Orangeville L, Houle D, Duchesne L. *et al.* Beneficial effects of climate warming on boreal tree growth may be transitory. *Nat Commun* 2018;**9**:3213. https://doi.org/10.1038/s41467-018-05705-4.

Fiore NM, Goulden ML, Czimczik CI. *et al.* Do recent NDVI trends demonstrate boreal forest decline in Alaska? *Environ Res Lett* 2020;**15**:095007. https://doi.org/10.1088/1748-9326/ab9c4c.

Forrester DI. Linking forest growth with stand structure: tree size inequality, tree growth or resource partitioning and the asymmetry of competition. *For Ecol Manage* 2019;**447**:139–57. https://doi.org/10.1016/j.foreco.2019.05.053.

Gardiner B, Moore J. Creating the wood supply of the future. In: Fenning T, ed. *Challenges and Opportunities for the World's Forests in the 21st Century*. Netherlands: Springer, 2014; 677–704.

Gauthier S, Bernier P, Kuuluvainen T. *et al.* Boreal forest health and global change. *Science* 2015;**349**:819–22. https://doi.org/10.1126/science.aaa9092.

Gillis MD, Omule AY, Brierley T. Monitoring Canada's forests: The National Forest Inventory. *For Chron* 2005;**81**:214–21. https://doi.org/10.5558/tfc81214-2.

Girardin MP, Bouriaud O, Hogg EH. *et al.* No growth stimulation of Canada's boreal forest under half-century of combined warming and CO_2 fertilization. *Proc Natl Acad Sci U S A* 2016a;**113**:E8406–14. https://doi.org/10.1073/pnas.1610156113.

Girardin MP, Guo XJ, Bernier PY. *et al.* Changes in growth of pristine boreal North American forests from 1950 to 2005 driven by landscape demographics and species traits. *Biogeosciences* 2012;**9**: 2523–36. https://doi.org/10.5194/bg-9-2523-2012.

Girardin MP, Hogg EH, Bernier PY. *et al.* Negative impacts of high temperatures on growth of black spruce forests intensify with the anticipated climate warming. *Glob Chang Biol* 2016b;**22**:627–43. https://doi.org/10.1111/gcb.13072.

Gomez C, White J, Wulder M. *et al.* Integrated object-based spatiotemporal characterization of forest change from an annual time series of Landsat image composites. *Can J Remote Sens* 2015;**41**: 271–92. https://doi.org/10.1080/07038992.2015.1089162.

Hansen MJ, Franklin SE, Woudsma C. *et al.* Forest structure classification in the North Columbia mountains using the Landsat TM tasseled cap wetness component. *Can J Remote Sens* 2001;**27**:20–32. https://doi.org/10.1080/07038992.2001.10854916.

Harper K, Bergeron Y, Drapeau P. *et al.* Structural development following fire in black spruce boreal forest. *For Ecol Manage* 2005;**206**: 293–306. https://doi.org/10.1016/j.foreco.2004.11.008.

Harper K, Bergeron Y, Gauthier S. *et al.* Post-fire development of canopy structure and composition in black spruce forests of Abitibi, Québec: a landscape scale study. *Silva Fenn* 2002;**36**:249–263. https://doi.org/10.14214/sf.561.

Harper K, Boudreault C, DeGrandpré L. *et al.* Structure, composition, and diversity of old-growth black spruce boreal forest of the Clay Belt region in Quebec and Ontario. *Environ Rev* 2003;**11**:S79–98. https://doi.org/10.1139/a03-013.

Hartigan JA, Wong MA. *et al.* A k-means clustering algorithm. *Appl Stat* 1979;**28**:100–8. https://doi.org/10.2307/2346830.

Hastie T, Tibshirani R, Friedman JH. *et al. The Elements of Statistical Learning: Data Mining, Inference, and Prediction Vol 2*. New York, New York: Springer, 2009.

Hayden, J. *Ontario Forest Growth and Yield Program Field Manual for Establishing and Measuring Permanent Sample Plots*. Ministry of Natural Resources, 1995. Sault Ste. Marie, Ontario: Ontario Forest Research Institute. https://books.google.ca/books?id=gZKvAAAACAAJ.

Hermosilla T, Wulder MA, White JC. *et al.* An integrated Landsat time series protocol for change detection and generation of annual gap-free surface reflectance composites. *Remote Sens Environ* 2015;**158**:220–34. https://doi.org/10.1016/j.rse.2014.11.005.

Hermosilla T, Wulder MA, White JC. *et al.* Mass data processing of time series Landsat imagery: pixels to data products for forest monitoring. *Int J Digit Earth* 2016;**9**:1035–54. https://doi.org/10.1080/17538947.2016.1187673.

Huang J, Tardif JC, Bergeron Y. *et al.* Radial growth response of four dominant boreal tree species to climate along a latitudinal gradient in the eastern Canadian boreal forest. *Glob Chang Biol* 2010;**16**: 711–31. https://doi.org/10.1111/j.1365-2486.2009.01990.x.

Hussain A, Classens G, Guevara-Rozo S. *et al.* Spatial variation in soil available water holding capacity alters carbon mobilization and allocation to chemical defenses along jack pine stems. *Environ Exp Bot* 2020;**171**:103902. https://doi.org/10.1016/j.envexpbot.2019.103902.

Johnstone JF, McIntire EJB, Pedersen EJ. *et al.* A sensitive slope: estimating landscape patterns of forest resilience in a changing climate. *Ecosphere* 2010;**1**:1–21. https://doi.org/10.1890/ES10-00102.1.

Kane VR, Gillespie AR, McGaughey R. *et al.* Interpretation and topographic compensation of conifer canopy self-shadowing. *Remote Sens Environ* 2008;**112**:3820–32. https://doi.org/10.1016/j.rse.2008.06.001.

Kane VR, McGaughey RJ, Bakker JD. *et al.* Comparisons between field- and LiDAR-based measures of stand structural complexity. *Can J For Res* 2010;**40**:761–73. https://doi.org/10.1139/X10-024.

Key CH, Benson NC. Landscape assessment (LA) sampling and analysis methods. In: Lutes DC, Keane RE, Caratti JF. *et al.*, eds. *FIREMON: Fire Effects Monitoring and Inventory System*. Ogden, UT: USDA Forest Service, Rocky Mountain Research Station, 2006.

Kurz WA, Stinson G, Rampley GJ. *et al.* Risk of natural disturbances makes future contribution of Canada's forests to the global carbon cycle highly uncertain. *PNAS* 2008;**105**:1551–5. https://doi.org/10.1073/pnas.0708133105.

Lefsky MA, Cohen WB, Parker GG. *et al.* LiDAR Remote Sensing for Ecosystem Studies: LiDAR, an emerging remote sensing technology that directly measures the three-dimensional distribution of plant canopies, can accurately estimate vegetation structural attributes and should be of particular interest to forest, landscape, and global ecologists. *Bioscience* 2002;**52**:19–30. https://doi.org/10.1641/0006-3568(2002)052[0019:LRSFES]2.0.CO;2.

Mahony CR, Wang T, Hamann A. *et al.* A global climate model ensemble for downscaled monthly climate normals over North

America. *Int J Climatol* 2022;**42**:5871–91. https://doi.org/10.1002/joc.7566.

Mamet SD, Chun KP, Metsaranta JM. *et al.* Tree rings provide early warning signals of jack pine mortality across a moisture gradient in the southern boreal forest. *Environ Res Lett* 2015;**10**:084021. https://doi.org/10.1088/1748-9326/10/8/084021.

Marchand W, Girardin MP, Hartmann H. *et al.* Taxonomy, together with ontogeny and growing conditions, drives needleleaf species' sensitivity to climate in boreal North America. *Glob Chang Biol* 2019;**25**:2793–809. https://doi.org/10.1111/gcb.14665.

Matasci G, Hermosilla T, Wulder MA. *et al.* Large-area mapping of Canadian boreal forest cover, height, biomass and other structural attributes using Landsat composites and LiDAR plots. *Remote Sens Environ* 2018;**209**:90–106. https://doi.org/10.1016/j.rse.2017.12.020.

Mazerolle MJ. *AICcmodavg: Model selection and multimodel inference based on (Q)AIC(c). R package version 2.3–1*. 2020. https://cran.r-project.org/package=AICcmodavg.

McDowell NG, Allen CD, Anderson-Teixeira K. *et al.* Pervasive shifts in forest dynamics in a changing world. *Science* 2020;**368**:eaaz9463.

MNRF. *Forest Health Conditions in Ontario 2001*. Ottawa, Ontario: Ministry of Northern Development, Mines, Natural Resources and Forestry, 2001, 20. https://www.ontario.ca/files/2022-07/mnrf-srb-forest-health-conditions-ontario-2021-en-2022-07-20.pdf.

MNRF. *Growth and Yield Program - PSP and PGP Reference Manual*. Ontario Ministry of Natural Resources and Forestry, 2016; 677. Ottawa, Ontario.

Moan MÅ, Noordermeer L, White JC. *et al.* Detecting and excluding disturbed forest areas improves site index determination using bitemporal airborne laser scanner data. *Forestry* 2023. https://doi.org/10.1093/forestry/cpad025.

Moran PA. Notes on continuous stochastic phenomena. *Biometrika* 1950;**37**:17–23. https://doi.org/10.1093/biomet/37.1-2.17.

Moreau G, Chagnon C, Achim A. *et al.* Opportunities and limitations of thinning to increase resistance and resilience of trees and forests to global change. *Forestry* 2022;**95**:595–615.

Oliver CD, Larson BC. *Forest Stand Dynamics*. New York: Wiley, 1996.

Olofsson P, Foody GM, Herold M. *et al.* Good practices for estimating area and assessing accuracy of land change. *Remote Sens Environ* 2014;**148**:42–57. https://doi.org/10.1016/j.rse.2014.02.015.

Pan Y, Birdsey RA, Fang J. *et al.* A large and persistent carbon sink in the world's forests. *Science* 2011;**333**:988–93. https://doi.org/10.1126/science.1201609.

Peng C, Ma Z, Lei X. *et al.* A drought-induced pervasive increase in tree mortality across Canada's boreal forests. *Nature Clim Change* 2011;**1**:467–71. https://doi.org/10.1038/nclimate1293.

Powell SL, Cohen WB, Healey SP. *et al.* Quantification of live aboveground forest biomass dynamics with Landsat time-series and field inventory data: a comparison of empirical modeling approaches. *Remote Sens Environ* 2010;**114**:1053–68. https://doi.org/10.1016/j.rse.2009.12.018.

Queinnec M, Coops NC, White JC. *et al.* Mapping dominant boreal tree species groups by combining area-based and individual tree crown LiDAR metrics with Sentinel-2 data. *Can J Remote Sens* 2022a;**49**:1–19.

Queinnec M, Coops NC, White JC. *et al.* Developing a forest inventory approach using airborne single photon LiDAR data: from ground plot selection to forest attribute prediction. *Forestry* 2022b;**95**:347–62. https://doi.org/10.1093/forestry/cpab051.

Régnière J, Saint-Amant R, Béchard A. *et al. BioSIM 11–Manuel d'utilisation*. Quebec, QC: Natural Resources Canada, Canadian Forest Services, Laurentian Forestry Center, 2017.

Roberts DR, Bahn V, Ciuti S. *et al.* Cross-validation strategies for data with temporal, spatial, hierarchical, or phylogenetic structure. *Ecography* 2017;**40**:913–29. https://doi.org/10.1111/ecog.02881.

Rogers BM, Solvik K, Hogg EH. *et al.* Detecting early warning signals of tree mortality in boreal North America using multiscale satellite data. *Glob Change Biol* 2018;**24**:2284–304. https://doi.org/10.1111/gcb.14107.

Sánchez-Pinillos M, D'Orangeville L, Boulanger Y. *et al.* Sequential droughts: a silent trigger of boreal forest mortality. *Glob Chang Biol* 2022;**28**:542–56. https://doi.org/10.1111/gcb.15913.

Seidl R, Schelhaas M-J, Rammer W. *et al.* Increasing forest disturbances in Europe and their impact on carbon storage. *Nature Clim Change* 2014;**4**:806–10. https://doi.org/10.1038/nclimate2318.

Seidl R, Thom D, Kautz M. *et al.* Forest disturbances under climate change. *Nature Clim Change* 2017;**7**:395–402. https://doi.org/10.1038/nclimate3303.

Sen PK. Estimates of the regression coefficient based on Kendall's tau. *J Am Stat Assoc* 1968;**63**:1379–89. https://doi.org/10.1080/01621459.1968.10480934.

Shapiro SS, Wilk MB. An analysis of variance test for normality (complete samples). *Biometrika* 1965;**52**:591–611. https://doi.org/10.1093/biomet/52.3-4.591.

Smirnova E, Bergeron Y, Brais S. Influence of fire intensity on structure and composition of jack pine stands in the boreal forest of Quebec: Live trees, understory vegetation and dead wood dynamics. *For Ecol Manage* 2008;**255**:2916–27. https://doi.org/10.1016/j.foreco.2008.01.071.

Stehman S. Statistical Rigor and Practical Utility in Thematic Map Accuracy Assessment. *Photogramm Eng Remote Sensing* 2001;**67**:727–34.

Subedi N, Sharma M. Climate-diameter growth relationships of black spruce and jack pine trees in boreal Ontario, Canada. *Glob Chang Biol* 2013;**19**:505–16. https://doi.org/10.1111/gcb.12033.

Sulla-Menashe D, Woodcock CE, Friedl MA. Canadian boreal forest greening and browning trends: an analysis of biogeographic patterns and the relative roles of disturbance versus climate drivers. *Environ Res Lett* 2018;**13**:014007. https://doi.org/10.1088/1748-9326/aa9b88.

Theil H. A rank-invariant method of linear and polynomial regression analysis. *Indag Math* 1950;**12**:173.

Tucker CJ. Red and photographic infrared linear combinations for monitoring vegetation. *Remote Sens Environ* 1979;**8**:127–50. https://doi.org/10.1016/0034-4257(79)90013-0.

Urquizo N, Bastedo J, Brydges T. *et al. Ecological Assessment of the Boreal Shield Ecozone*. Ottawa, Ontario: Environment Canada, 2000, 90. https://publications.gc.ca/collections/collection_2014/ec/En40-600-2000-eng.pdf.

Valavi R, Elith J, Lahoz-Monfort JJ. *et al.* blockCV: An r package for generating spatially or environmentally separated folds for k-fold cross-validation of species distribution models. *Methods Ecol Evol* 2018;**10**:225–232.

Verbyla AP. Modelling variance heterogeneity: residual maximum likelihood and diagnostics. *J R Stat Soc B Methodol* 1993;**55**:493–508.

Vicente-Serrano SM, Beguería S, López-Moreno JI. A multiscalar drought index sensitive to global warming: the standardized precipitation evapotranspiration index. *J Climate* 2010;**23**:1696–718. https://doi.org/10.1175/2009JCLI2909.1.

Vogelmann JE, Gallant AL, Shi H. *et al.* Perspectives on monitoring gradual change across the continuity of Landsat sensors using

time-series data. *Remote Sens Environ* 2016;**185**:258–70. https://doi.org/10.1016/j.rse.2016.02.060.

Wang T, Hamann A, Spittlehouse D. *et al.* Locally downscaled and spatially customizable climate data for historical and future periods for North America. *PloS One* 2016;**11**:e0156720. https://doi.org/10.1371/journal.pone.0156720.

Wester M, Henson B, Crins W. *et al. The Ecosystems of Ontario, Part 2: Ecodistricts*. Peterborough, Ontario: Science and Research Technical Report-Ontario Ministry of Natural Resources and Forestry, TR-26, 2018.

White JC, Wulder MA, Hermosilla T. *et al.* A nationwide annual characterization of 25 years of forest disturbance and recovery for Canada using Landsat time series. *Remote Sens Environ* 2017;**194**:303–21. https://doi.org/10.1016/j.rse.2017.03.035.

White JC, Wulder MA, Hobart GW. *et al.* Pixel-based image compositing for large-area dense time series applications and science. *Can J Remote Sens* 2014;**40**:192–212. https://doi.org/10.1080/07038992.2014.945827.

Wotherspoon, A., Burnett, M., Bernard, A., Achim, A., Coops, N. C. *Climate Scenarios for Canadian Forests*. 2022. https://doi.org/10.13140/RG.2.2.18449.92009.

Wulder MA, Hermosilla T, White JC. *et al.* Biomass status and dynamics over Canada's forests: disentangling disturbed area from associated aboveground biomass consequences. *Environ Res Lett* 2020;**15**:094093. https://doi.org/10.1088/1748-9326/ab8b11.

Wulder MA, Roy DP, Radeloff VC. *et al.* Fifty years of Landsat science and impacts. *Remote Sens Environ* 2022;**280**:113195. https://doi.org/10.1016/j.rse.2022.113195.

Wulder MA, White JC, Nelson RF. *et al.* LiDAR sampling for large-area forest characterization: a review. *Remote Sens Environ* 2012;**121**:196–209. https://doi.org/10.1016/j.rse.2012.02.001.

Zald HSJ, Wulder MA, White JC. *et al.* Integrating Landsat pixel composites and change metrics with LiDAR plots to predictively map forest structure and aboveground biomass in Saskatchewan, Canada. *Remote Sens Environ* 2016;**176**:188–201. https://doi.org/10.1016/j.rse.2016.01.015.